UNIVERSITI TEKNOLOGI MARA
Cawangan Kedah
Kampus Sungai Petani

2021 iCMS
INTERNATIONAL CONFERENCE ON COMPUTING, MATHEMATICS AND STATISTICS

e-PROCEEDINGS

of The 5th International Conference on Computing, Mathematics and Statistics (iCMS2021)

4-5 August 2021

Driving Research Towards Excellence

e-Proceedings
of the 5th International Conference on Computing, Mathematics and Statistics (iCMS 2021)

Driving Research Towards Excellence

Editor-in-Chief: Norin Rahayu Shamsuddin

Editorial team:

Dr. Afida Ahamad
Dr. Norliana Mohd Najib
Dr. Nor Athirah Mohd Zin
Dr. Siti Nur Alwani Salleh
Kartini Kasim
Dr. Ida Normaya Mohd Nasir
Kamarul Ariffin Mansor

e-ISBN: 978-967-2948-12-4
DOI

Library of Congress Control Number:

Publication by
Department of Mathematical Sciences
Faculty of Computer & Mathematical Sciences
UiTM Kedah

TABLE OF CONTENT

PART 1: MATHEMATICS

PART 2: STATISTICS

PART 3: COMPUTER SCIENCE & INFORMATION TECHNOLOGY

PART 4: OTHERS

RADIATIVE CASSON FLUID OVER A SLIPPERY VERTICAL RIGA PLATE WITH VISCOUS DISSIPATION AND BUOYANCY EFFECTS

Siti Khuzaimah Soid[1], Khadijah Abdul Hamid[2], Ma Nuramalina Nasero[3], NurNajah Nabila Abdul Aziz[4]
[1,2,3,4] Faculty of Computer and Mathematical Sciences, University Teknologi MARA, 40450 UiTM Shah Alam, Selangor, Malaysia
([1] khuzaimah@tmsk.uitm.edu.my, [2] khadijah@tmsk.uitm.edu.my, [3] manuramalina@gmail.com, [4] Najahnabila0505@gmail.com)

The application of Casson fluid such as concentrated fruit juice and tomato sauce might involve problems during the manufacturing process to maintain their high quality. This study aims to investigate the radiative Casson fluid in the presence of the magnetic field, velocity slip, thermal slip, viscous dissipation and buoyancy effects over permeable slippery vertical Riga stretching and shrinking plates. The governing partial differential equations are translated into ordinary differential equations using similarity transformation. The equations are then solved numerically using a boundary value problem solver (BVP4C) in MATLAB software. The skin friction coefficient and the heat transfer rate are significantly influenced by the Casson fluid and the modified Hartmann number which both coefficients increase for stretching and shrinking plates. Concurrently, their fluid flows increase while heat distributions decrease in the boundary layer for both plates. This theoretical research becomes a benchmark for the food industry especially in producing canned food.
***Keywords*:** Casson fluid, Riga plate, viscous dissipation, buoyancy effect

1. Introduction

The non-Newtonian fluid is a complex fluid for which the shearing stress is not related to the rate of shearing strain. The fluid's viscosity depends on the shear rate, either contributing to shear thickening, which is the rise in the viscosity of non-Newtonian, or shear thinning, indicating the decrease in the viscosity of non-Newtonian. Casson fluid is one of the non-Newtonian fluids. It has its characteristics which behave like an elastic solid which no flow occurs with small shear stress (Alwawi et al., 2019). The examples are concentrated fruit juices, tomato sauce, honey, sewage sludge, blood and jelly (Ullah et al., 2017). An analysis related to the Casson fluid was conducted by Haldar et al. (2018) where they studied on the steady boundary layer flow and heat transfer in Casson fluid over an exponentially permeable shrinking sheet with convective boundary condition. The study was found that wall temperature declines with the increasing values of convective parameter. An important use of Casson fluid is to provide adequate lubrication of moving system components with the presence of water resistance for example a submarine. Many references can be captured in the detailed explanations (Awais et al., 2021; Anwar et al., 2021).

The heat transfer over a stretching/shrinking sheet is a critical investigation due to its wide range of applications in the industrial and engineering fields. Paper production, glass blowing, metal sheet cooling, jet emerging from slot-jets, and flow over the submarine tips are some of these applications (Vajravelu and Mukhopadhyay, 2015). Crane (1970) first introduced fluid flow past a stretching sheet, which an exact analytical solution to the equation of the boundary layer was studied. Meanwhile, Wang (1990) researched the boundary layer flow over a shrinking board, where an unstable shrinking film solution was addressed. The shrinking plate has a reverse flow in the boundary layer that would create a complexity. There are two conditions where the solutions of the fluid flow towards the shrinking case is possible to exist, having an adequate suction imposed on the plate or creating a stagnation flow or both (Lok et al., 2011). There are various researchers explored the fluid flow towards Casson fluid on both plates (Lund et al., 2020; Mousavi et al., 2021; Makinde, 2021).

The viscous dissipation is also an important subject to be discussed as they are responsible for the instability during the process of heat transfer. In other words, viscous dissipation is an internal process for heat generation that can lead to an unpredictable distribution of temperature (Requile, 2020). Hussanan et al. (2016) said viscous dissipation is a process in which the work is done by a fluid on an adjacent layer due to the action of shear forces. The combination of permanent magnets and a span-aligned series of alternating electrodes placed on a flat surface is the electromagnetic actuator with the stated name, Riga plate. Riga plate is used as an important agent to minimize the skin friction and pressure drag for instance surfaces of submarine, aerofoil, and battle tank. One of the researches done by Iqbal et al. (2018) stated that viscous dissipation enables to enhance fluid temperature which contribute in lowering the rate of heat transfer on the surface. They did research on stagnation point flow of Casson fluid over a Riga plate of variable thickness. A huge number of researches have been performed on viscous dissipation effects over Riga plate (Nayak et al., 2019; Yusof et al., 2020; Eldabe et al., 2021). Motivated from the above literature, this study investigates the viscous dissipation on Casson fluid over a vertical Riga plate with consideration of radiation and buoyancy effects due to their natural influences in many systems.

2. Mathematical Formulation

The mathematical formulation of the governing boundary layer equations for mass, momentum and thermal energy conservation has been discussed in this review. The stagnation flow of a slippery radiative Casson fluid over an exponentially Riga plate placed vertically is modeled as the equations below (Haldar at el., 2018).

Continuity Equation:

$$\frac{\partial u}{\partial x}+\frac{\partial v}{\partial y}=0 \tag{1}$$

Momentum Equation:

$$u\frac{\partial u}{\partial x}+v\frac{\partial u}{\partial y}=u_e\frac{\partial u_e}{\partial x}+\upsilon\left(1+\frac{1}{B}\right)\frac{\partial^2 u}{\partial y^2}+\frac{\pi j_o M}{8\rho}e^{\left(\frac{\pi}{\alpha_1}y\right)}+g\beta\left(T-T_\infty\right) \tag{2}$$

Energy Equation:

$$u\frac{\partial T}{\partial x}+v\frac{\partial T}{\partial y}=\alpha\frac{\partial^2 T}{\partial y^2}+\frac{16\sigma^* T_\infty^3}{3k^*\rho C_p}\frac{\partial^2 T}{\partial y^2}+\frac{\mu}{\rho C_p}\left(1+\frac{1}{B}\right)\left(\frac{\partial u}{\partial y}\right)^2 \tag{3}$$

Boundary Conditions:

$$\begin{gathered}u=\lambda u_w\left(x\right)+N\frac{\partial u}{\partial y},\quad v=-V_w\left(x\right),\quad T=T_w+D\frac{\partial T}{\partial y}\ \text{at}\ y=0\\ u\to u_e\left(x\right),\ T\to T_\infty,\quad \text{as}\ \ y\to\infty\end{gathered} \tag{4}$$

where u and v are the components of velocity in the x and y directions respectively, υ is the kinematic viscosity, β is coefficient of volume expansion, ρ is fluid density, g is acceleration due to gravity, μ is viscosity. It is assumed that $u=\lambda u_w\left(x\right)+N\left(\partial u/\partial y\right)$ is the surface velocity with λ

be the constant stretching/shrinking parameter where $\lambda > 0$ refers to stretching and $\lambda < 0$ refers to shrinking sheets. The wall velocity $u_w(x) = U_0 e^{x/L}$, where U_0 is the reference velocity and the velocity slip coefficient $N = N_1 e^{x/2L}$ in which N_1 is the original velocity slip value. However, the straining velocity $u_e(x) = U_0 e^{x/L}$ shows the flow velocity far from the sheet surface (inviscid flow). Next, $V_w(x) = V_0 e^{x/2L}$ is the surface velocity where V_0 is the initial force with $V_0 > 0$ is for injection and $V_0 < 0$ is for suction. Meanwhile, the thermal slip factor $D = D_1 e^{x/2L}$ in which D_1 is the initial value of the thermal slip factor. The parameter T is the fluid temperature, $T_w = T_\infty + T_0 e^{x/2L}$ is the sheet temperature where the ambient constant temperature is T_∞ and the reference temperature is T_0. $M = M_0 e^{2x/L}$ is a variable of magnetic field where M_0 is a constant, j_0 is the applied current density in the electrodes and α_1 is the width for electrodes and magnets (Nasir et al., 2019). C_p is the specific heat at constant pressure and $\alpha = k / \rho C_p$ is the thermal diffusivity where k is the thermal conductivity. The Rosseland approximation for the radiative heat flux is simplified as $q_r = -(4\sigma^* / 3k^*)(\partial T^4 / \partial y)$ where σ^* is the Stefan–Boltzman constant and k^* is the absorption coefficient as depicted in (2). It is assumed that the temperature differences within the flow are sufficiently small so that T^4 can be expressed as a linear function of temperature in a Taylor series about T_∞ and neglecting the higher terms which is given by (Alavi et al., 2017)

$$T^4 \cong 4T_\infty^3 T - 3T_\infty^4. \tag{5}$$

Using the following similarity variables η, the velocity components u, v and the dimensionless temperature θ can be considered in (1) - (3):

$$\psi = \sqrt{2U_0 \upsilon L}\, e^{\frac{x}{2L}} f(\eta), \qquad \theta(\eta) = \frac{T - T_\infty}{T_w - T_\infty} \qquad \eta = \sqrt{\frac{U_0}{2\upsilon L}}\, e^{\frac{x}{2L}} y \tag{6}$$

and the dimensionless stream function ψ is defined by

$$u = \frac{\partial \psi}{\partial y} \text{ and } \quad v = -\frac{\partial \psi}{\partial x}. \tag{7}$$

The similarity variables (6) are substituted into (1) – (3) which reduce into the following ordinary differential equations as below:

Momentum Equation:

$$\left(1 + \frac{1}{B}\right) f'''(\eta) + 2 - 2f'^2(\eta) + f(\eta) f''(\eta) + 2Qe^{(-A\eta)} + 2\sigma\theta = 0 \tag{8}$$

Energy Equation:

$$\left(1 + \frac{4}{3}Rd\right)\theta''(\eta) + \Pr\theta'(\eta) f(\eta) - \Pr f'(\eta)\theta(\eta) + Ec\left(1 + \frac{1}{B}\right) f''^2(\eta) = 0 \tag{9}$$

with the boundary conditions:

$$f'(0)=\lambda+\omega f''(0), \quad f(0)=S, \quad \theta(0)=1+\varepsilon\theta'(0)$$
$$f'(\infty)\to 1, \quad \theta(\infty)\to 0 \quad \text{as} \quad y\to\infty. \tag{10}$$

The primes are denoted as differentiation with respect to η, B is the Casson parameter, Q is the modified Hartmann number, A is the dimensionless parameter, σ is the buoyancy parameter, Rd is the radiation parameter, $\Pr$ is the Prandtl number, Ec is the Eckert number, ω is the velocity slip factor, S is the suction/injection parameter which $S>0$ for suction and $S<0$ for injection, ε is the thermal slip factor. The quantities of physical interest in this problem are the skin friction coefficient and the local Nusselt number which are defined as:

$$C_f = \frac{\tau_w}{\rho u_w^2(x)}, \qquad Nu = \frac{x\, q_w}{k(T_w - T_\infty)} \tag{11}$$

The wall shear stress, τ_w at the surface is given as

$$\tau_w = \left(\mu + \frac{p_y}{\sqrt{2\pi_c}}\right)\left(\frac{\partial u}{\partial y}\right)_{y=0} \tag{12}$$

where p_y is yield stress , π_c is the critical value of product of deformation rate component and the rate of heat transfer at the wall is given by

$$q_w = -k\left(1+(4/3)Rd\right)\left(\partial T/\partial y\right)_{y=0}. \tag{13}$$

Substituting (6) and (13) into (12), the new physical quantities are reduced as

$$\sqrt{\frac{2L}{x}}\frac{\sqrt{\mathrm{Re}}}{\left(1+\frac{1}{B}\right)}C_f = f''(0), \qquad \frac{Nu}{\sqrt{\frac{x}{2L}}\sqrt{\mathrm{Re}}\left(1+\frac{4}{3}Rd\right)} = -\theta'(0) \tag{14}$$

where L is characteristic length and $\mathrm{Re}=xu_w(x)/\upsilon$ is the local Reynolds number.

3. Results and Discussion

The numerical computations were executed for the pertinent parameters considered in this research where the boundary condition $\eta\to\infty$ was fixed $\eta=10$. The comparison results for the non-buoyancy effect with Haldar et al. (2018) and Yusof et al. (2020) are found in good agreement as shown in Table 1. Overall, the local Nusselt number, $-\theta'(0)$ is noticed to increase as the Casson parameter B increases for the thermal slip parameter $\varepsilon=3.33$ and the shrinking sheet $\lambda=-1$. It is noticed that there are slightly different in results between the present and the previous studies. It might due to the usage of different versions in MATLAB. It is considered the numerical results obtained are correct and reliable.

Table 1: Comparison of heat transfer coefficient, $-\theta'(0)$ for the various value of B as $Q = Rd = Ec = A = \omega = 0$, $S = 5.0$, $\varepsilon = 3.33$, $\Pr = 0.7$, $\lambda = -1.0$ and $\sigma = 0.0$.

ε	B	Haldar at el. (2018)	Yusof et al. (2020)	Present study
3.33	1.0	0.2755	0.2755	0.2763
	1.4	0.2756	0.2756	0.2764
	2.0	0.2756	0.2756	0.2766
	2.4	0.2756	0.2756	0.2766

Further analysis on the behavior of the velocity profiles and the temperature profiles for different physical parameters are examined. The skin friction and the heat transfer rate values are also reported. The whole discussion considered the buoyancy effect specifically on the assisting flow $\sigma = 0.2$ for both stretching and shrinking plates with $\lambda = 1$ and $\lambda = -1$, respectively. The Casson parameter, modified Harman number and suction/injection parameter are varied while the dimensionless parameter A, the radiation parameter Rd, the Prandtl number $\Pr$, the Eckert number Ec, the velocity slip factor ω and the thermal slip factor ε are fixed to 1 throughout the discussion.

Table 2: Skin friction coefficient $f''(0)$ and local Nusselt Number $-\theta'(0)$ for different values of B when $Q = Rd = Ec = A = \omega = S = \Pr = \varepsilon = 1, \sigma = 0.2$ for $\lambda = -1$ and 1.

λ	B	$f''(0)$	$-\theta'(0)$
-1	1	1.44642945	0.31453586
	3	1.58940614	0.39861559
	5	1.62494292	0.41526553
	1000	1.68425844	0.43984523
1	1	0.16805332	0.53200768
	3	0.19405006	0.53362593
	5	0.20077725	0.53402820
	1000	0.21225288	0.53469730

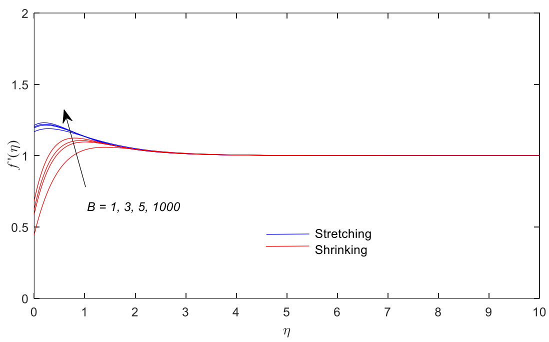

Figure 1: Velocity profile, $f'(\eta)$ for various values of B when $Q = Rd = Ec = A = \omega = S = \Pr = \varepsilon = 1, \sigma = 0.2$ for $\lambda = 1$ (stretching) and $\lambda = -1$ (shrinking).

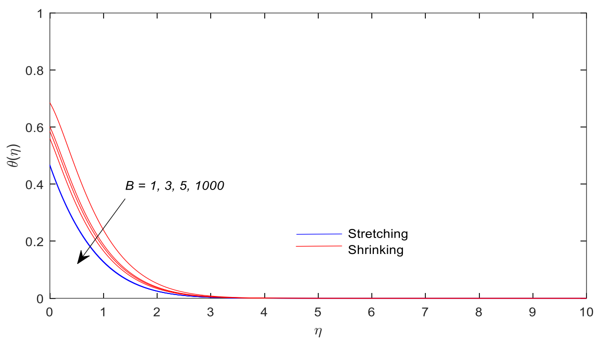

Figure 2: Temperature profile, $\theta(\eta)$ for various values of B when $Q = Rd = Ec = A = \omega = S = \Pr = \varepsilon = 1, 1, \sigma = 0.2$ for $\lambda = 1$ (stretching) and $\lambda = -1$ (shrinking).

Table 2 shows the effects of the Casson parameter B for both $\lambda = 1$ and $\lambda = -1$ when $Q = Rd = Ec = A = \omega = S = \Pr = \varepsilon = 1$ and $\sigma = 0.2$. It is noticed that the values of the skin friction coefficient, $f''(0)$ and the local Nusselt number, $-\theta'(0)$ become greater for both stretching and shrinking plates as the Casson parameter increases. The drag force and the heat transfer rate have maximum values when the Casson parameter approaches infinity. In fact, as the Casson parameter approaches infinity, the Casson fluid (non-Newtonian) becomes a regular fluid (Newtonian). It means that the rate of the shear stress and the heat dispersion on the surface are greater for Newtonian fluid compared to the non-Newtonian fluid, particularly for Casson fluid.

Figures 1 and 2 indicate the velocity and the temperature behavior in the boundary layer, respectively. As the Casson fluid parameter B increases, the fluid velocity increases when the plate is stretched and shrunk, respectively with the ratio of one. It implies that the fluid travels faster in the boundary layer initially and it starts to slow down when the fluid adjacent to the inviscid flow. An opposite analysis can be concluded for the temperature profile where the fluid temperature decreases as the Casson parameter increases. It is highlighted, the boundary layer thickness decelerates for both velocity and temperature profiles which the thickness is thinner for the stretching plate compared to the shrinking plate. This is due to the Casson fluid's high viscosity, where it flows steadily at a steady speed for a stretching plate than a shrinking plate. Apparently, Casson fluid does affect the fluid flow and the heat transfer especially on the shrinking surface rather than on the stretching surface.

Table 3: Skin friction coefficient, $f''(0)$ and local Nusselt number $-\theta'(0)$, for different values Q and λ when Rd = Pr = Ec = A = ω = S = B = 1 and ε = 1.

λ	Q	$f''(0)$	$-\theta'(0)$
-1.0	0.5	1.35277636	0.30396290
	2.5	1.69979144	0.32938878
	4.5	1.99302104	0.32663310
1.0	0.5	0.09264741	0.52814975
	2.5	0.37861293	0.53509000
	4.5	0.63159076	0.52633580

Table 3 reveals the skin friction coefficient, $f''(0)$ and the local Nusselt number, $-\theta'(0)$ with a certain value of the physical parameters that are Rd = Pr = Ec = S = ω = B = ε = A = 1 for the effects on the modified Hartmann number on both stretching and shrinking plates. The skin friction coefficient increases for both plates. Surprisingly, there is an inconsistency in the heat dispersed even though the Hartman number Q keeps increasing. The value of $-\theta'(0)$ is like a sinusoidal pattern. This might due to the character of the Riga plate itself which produces magnetic behavior that varies exponentially. The scenario of the velocity and thermal boundary layers can be captured from Figures 3 and 4. The velocity of the fluid $f'(\eta)$ increases. However, the temperature distribution $\theta(\eta)$ decreases for both stretching and shrinking plates as the Hartmann number increases. In other words, the modified Hartmann number, Q enables to increase the strength of the external electrical field leading to an increment in the distribution of velocity. However, the fluid temperature decreases resulting in the decrease in the thermal boundary layer thickness. This behaviour enables to accelerate the cooling process.

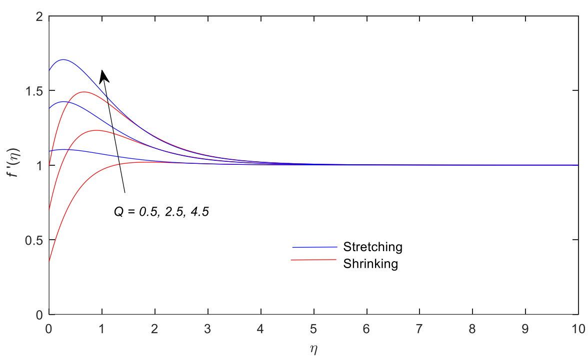

Figure 3: Velocity profile, $f'(\eta)$ for various values of Q when Rd= Pr = Ec = A = ω = S = B = ε = 1 for λ = 1 (stretching) and $\lambda = -1$ (shrinking).

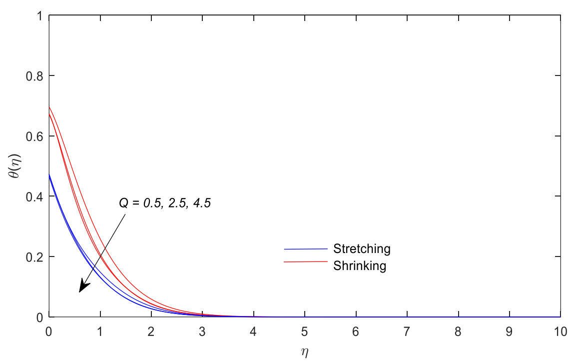

Figure 4: Temperature profile, $\theta(\eta)$ for various values of Q when Rd = Pr = Ec = A = ω = S = B = ε = 1 for $\lambda = 1$ (stretching) and $\lambda = -1$ (shrinking).

Table 4: Skin friction coefficient, $f''(0)$ and local Nusselt number $-\theta'(0)$, for different values S and λ when Rd = Pr = Ec = A = ω = Q = B = 1 and ε = 1.

λ	S	$f''(0)$	$-\theta'(0)$
-1.0	-2.0	1.15464862	-0.04630545
	0.0	1.36294349	0.19533344
	2.0	1.51754415	0.41634897
1.0	-2.0	0.18002435	0.33130890
	0.0	0.17396785	0.46706254
	2.0	0.16114898	0.58940549

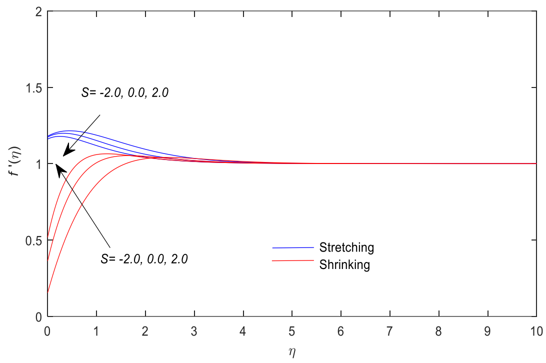

Figure 5: Velocity profile, $f'(\eta)$ for various values of S when Rd = Pr = Q = A = ω = Ec = B = ε = 1 for $\lambda = 1$ (stretching) and $\lambda = -1$ (shrinking).

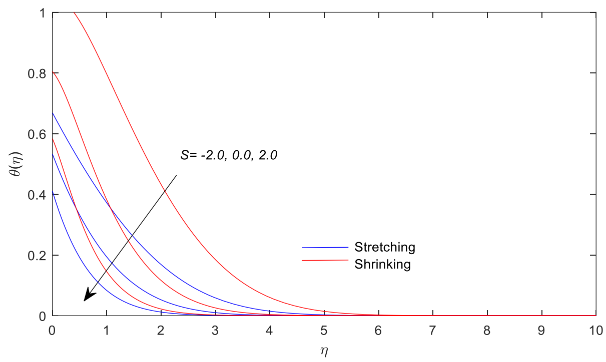

Figure 6: Temperature profile, $\theta(\eta)$ for various values of S when Rd = Pr = Q = A = ω = Ec = B = ε = 1 for $\lambda = 1$ (stretching) and $\lambda = -1$ (shrinking).

Table 4 demonstrates the skin friction coefficient, $f''(0)$ and the local Nusselt number, $-\theta'(0)$ when the fluid is sucked and injected on the surface with the strength of 2 for stretching and shrinking surfaces. The other physical parameters are fixed at Rd = Pr = Ec = B = Q = ω = ε = A =1. It is observed, the skin friction coefficient is lower when injection $S = -2.0$ is imposed but it is higher when suction $S = 2.0$ is imposed for shrinking plate and vice versa for the stretching plate. It means that, when the plate is shrunk, movement of the fluid on the surface decelerates caused by the effect of suction, whilst it accelerates for the effect of injection. A contradict pattern is observed when the plate is stretched. However, a consistent conclusion is viewed for the local Nusselt number for both shrinking and stretching plates which the rate of heat dispersed is minimum for injection and maximum for suction parameters. Unexpectedly, for the shrinking plate, the value of the local Nusselt number is negative for the injection case. This describes the heat is transferred from the fluid to the surface and simultaneously the scenario assists the movement of the fluid flow on the surface. The velocity and the temperature profiles are portrayed in Figures 5 and 6. The fluid velocity in the boundary layer increases for shrinking and decreases for stretching case from injection to suction. While the fluid temperature decreases in the boundary layer for both stretching and shrinking plates. The suction effect led to the thinning of the velocity and thermal boundary layer thicknesses as compared to the injection effect. These effects are dominant for shrinking plate compared to the stretching plate especially for velocity distribution. As can be concluded, the surface drag forced and the surface heat transfer values are highly affected when the plate is sucked rather than the plate is injected.

4. Conclusion

The problem of radiative Casson fluid in the presence of the magnetic field, velocity slip, thermal slip, viscous dissipation and buoyancy effects over a permeable slippery vertical Riga stretching and shrinking plates has been analyzed. The governing partial differential equations were transformed into ordinary differential equations using similarity transformation. The dimensionless equations were then solved numerically using a BVP4C embedded in MATLAB software. The Casson fluid and the modified Hartmann number influenced to increase the skin friction coefficient and the heat transfer rate for both stretching and shrinking surfaces. These two factors increased the fluid flow but decreased the heat distribution. The effect of suction was capable to decelerate the movement of the fluid on the surface while it accelerated for the effect of the injection. The rate of heat transfer was greater for suction rather than injection for both stretching and shrinking plates. The fluid velocity increased while the fluid temperature decreased in the boundary layer from injection to suction for both stretching and shrinking plates. Overall, the velocity boundary layer thickness was thicker but the thermal boundary layer thickness was thinner as Casson parameter or modified Hartman number was increased. The suction effect led to thinning the velocity and thermal boundary layer thicknesses compared to the injection effect.

Acknowledgment

The financial supports received from the Universiti Teknologi MARA are gratefully acknowledged.

References

Alavi, S.Q., Hussanan, A., Kasim, A.R.M., Rosli, N., and Salleh, M.Z. (2017). MHD stagnation point flow towards an exponentially stretching sheet with prescribed wall temperature and heat flux. *International Journal of Applied and Computational Mathematics,* 3 (4):3511-3523.

Alwawi, F.A., Alkasasbeh, H.T., Rashad, A.M., and Idris, R. (2019). Natural convection flow of Sodium Alginate based Casson nanofluid about a solid sphere in the presence of a magnetic field with constant surface heat flux. *Journal of Physic: Conference Series.* 1366.

Anwar, T., Kumam, P., and Watthayu, W. (2021). Unsteady MHD natural convection flow of Casson fluid incorporating thermal radiative flux and heat injection/suction mechanism under variable wall conditions. *Scientific Reports*, 11:1-15.

Awais. M., Raja, M. A. Z., Awan, S. E., Shoaib, M., and Ali, H. M. (2021). Heat and mass transfer phenomenon for the dynamics of Casson fluid through porous medium over shrinking wall subject to Lorentz force and heat source/sink. *Alexandria Engineering Journal*, 60(1):1355-1363.

Crane, L. J. (1970). Flow past a stretching plate. *Journal of Applied Mathematics and Physics (ZAMP)*, 21(4):645–647.

Eldabe, N.T., Gabr, M.E., Zaher, A.Z., and Zaher, S.A. (2021). The effect of Joule heating and viscous dissipation on the boundary layer flow of a magnetohydrodynamics micropolar-nanofluid over a stretching vertical Riga plate. *Heat Transfer*, 50(5):4788-4805.

Haldar, S., Mukhopadhyay, S., and Layek, G.C. (2018). Flow and heat transfer of Casson fluid over an exponentially shrinking permeable sheet in presence of exponentially moving free stream with convective boundary condition. *Mechanics of Advanced Materials and Structures*, 26 (17):1498-1504.

Hussanan, A., Salleh, M.Z., Khan, I., and Shafie, S. (2018). Analytical solution for suction and injection flow of a viscoplastic Casson fluid past a stretching surface in the presence of viscous dissipation. *Neural Computing and Applications*, 29:1507–1515.

Iqbal, Z., Azhar, E., Mehmood, Z., and Maraj, E.N. (2018). Unique outcomes of internal heat generation and thermal deposition on viscous dissipative transport of viscoplastic fluid over a Riga-plate. *Communications in Theoretical Physics*, 69(1):68-76.

Lok, Y.Y., Ishak, A., and Pop, I. (2011). MHD Stagnation-point flow towards a shrinking sheet. *International Journal Numerical Methods Heat Transfer Flow*, 21:61-72.

Lund, LA., Omar, Z., Khan, I., Sherif, E.S.M., and Abdo, H.S. (2020). Stability analysis of the magnetized Casson nanofluid propagating through an exponentially shrinking/stretching plate: dual solution. *Symmetry*, 12(7):1162.

Makinde, O.D., Awati, V.B., and Bujurke, N.M. (2021). Dirichlet series and closed-form exact solutions of MHD Casson fluid flow over a permeable stretching/ shrinking sheet. *Palestine Journal of Mathematics*, 10:109-119.

Mousavi, S.M., Rostami, M.N., Yousefi, M., Dinarvand, S., Pop, I., and Sheremet M.A. (2021). Dual solutions for Casson hybrid nanofluid flow due to a stretching/shrinking sheet: A new combination of theoretical and experimental models. *Chinese Journal of Physics*, 71:574-588.

Nasir, N. A. A. M., Ishak, A., and Pop, I. (2019). Stagnation point flow and heat transfer past a permeable stretching/shrinking Riga plate with velocity slip and radiation effects. *Journal of Zhejiang University-SCIENCE A*, 20:290–299.

Nayak, M. K., Shaw, S., Makinde, O. D., and Chamkha, A.J. (2019). Investigation of partial slip and viscous dissipation effects on the radiative tangent hyperbolic nanofluid flow past a vertical permeable Riga plate with internal heating: Bungiorno Model. *Journal of Nanofluids*, 8:51–62.

Requile, Y., Hirata, S.C., and Ouarzazi, M.N. (2020). Viscous dissipation effects on the linear stability of Rayleigh-Bénard-Poiseuille/Couette convection. *International Journal of Heat and Mass Transfer*, 146:118834(1)-118834(11).

Shateyi, S. (2008). Thermal radiation and buoyancy effects on heat and mass transfer over a semi-infinite stretching surface with suction and blowing. *Journal of Applied Mathematics*, 2008: 414830 (1)-414830 (13).

Ullah, I., Shafie, S., and Khan, I. (2017). Effects of slip condition and Newtonian heating on MHD flow of Casson fluid over a nonlinearly stretching sheet saturated in a porous medium. *Journal of King Saud University –Science*, 29:250-259.

Vajravelu, K., and Mukhopadhyay, S. (2015). *Fluid Flow, Heat and Mass Transfer at Bodies of Different Shapes: Numerical Solution*. New York: Elsevier Science.

Wang, C.Y. (1990). Liquid film on an unsteady stretching surface. *Quarterly of Applied Mathematics*, 48(4):601–610.

Yusof, N.S., Soid, S.K., Illias, M.R., Aziz, A.S.A., and Nasir, N.A.A.M. (2020). Radiative boundary layer flow of Casson fluid over an exponentially permeable slippery Riga plate with viscous dissipation. *Journal of Advanced Research in Applied Sciences and Engineering Technology*, 21 (1):41-51.

2021 ICMS

INTERNATIONAL CONFERENCE ON COMPUTING, MATHEMATICS AND STATISTICS

e ISBN 978-967-2948-12-4